

## RESEARCH ARTICLE

# Interregional causal influences of brain metabolic activity reveal the spread of aging effects during normal aging

Xin Di<sup>1,2</sup>  | Marie Wölfer<sup>1,3,4</sup> | Mario Amend<sup>5</sup> | Hans Wehrl<sup>5</sup> | Tudor M. Ionescu<sup>5</sup> | Bernd J. Pichler<sup>5</sup> | Bharat B. Biswal<sup>1,2</sup>  the Alzheimer's Disease Neuroimaging Initiative

<sup>1</sup>Department of Biomedical Engineering, New Jersey Institute of Technology, Newark, New Jersey

<sup>2</sup>School of Life Sciences and Technology, University of Electronic Science and Technology of China, Chengdu, China

<sup>3</sup>Clinical Affective Neuroimaging Laboratory (CANLAB), Otto-von-Guericke-University Magdeburg, Magdeburg, Germany

<sup>4</sup>Department for Behavioral Neurology, Leibniz Institute for Neurobiology, Magdeburg, Germany

<sup>5</sup>Werner Siemens Imaging Center, Department of Preclinical Imaging and Radiopharmacy, Eberhard Karls University Tuebingen, Tuebingen, Germany

## Correspondence

Bharat B. Biswal, Department of Biomedical Engineering, New Jersey Institute of Technology, 607 Fenster Hall, University Height, Newark, NJ 07102.  
Email: bbiswal@yahoo.com

## Funding information

Northern California Institute for Research and Education; Foundation for the National Institutes of Health; Canadian Institutes of Health Research; Transition Therapeutics; Takeda Pharmaceutical Company; Servier; Piramal Imaging; Pfizer Inc.; Novartis Pharmaceuticals Corporation; Neurotrack Technologies; NeuroRx Research; Meso Scale Diagnostics, LLC.; Merck & Co., Inc.; Lundbeck; Lumosity; Johnson & Johnson Pharmaceutical Research & Development, LLC.; Janssen Alzheimer Immunotherapy Research & Development, LLC.; IXICO Ltd.; GE Healthcare; Fujirebio US; Genentech, Inc.; F. Hoffmann-La Roche Ltd; EuroImmun; Eli Lilly and Company; Elan Pharmaceuticals, Inc.; Eisai Inc.; Cogstate; CereSpir, Inc.; Bristol-Myers Squibb Company; Biogen; BioClinica, Inc.; Araclon Biotech; Alzheimer's Drug Discovery Foundation; Alzheimer's Association; AbbVie; National Institute of Biomedical Imaging and Bioengineering; National Institute on Aging; Department of Defense, Grant/Award Number: W81XWH-12-2-0012; National Institutes of Health, Grant/Award Numbers: R01DA038895, R01AT009829, U01 AG024904; Alzheimer's Disease Neuroimaging Initiative

## Abstract

During healthy brain aging, different brain regions show anatomical or functional declines at different rates, and some regions may show compensatory increases in functional activity. However, few studies have explored interregional influences of brain activity during the aging process. We proposed a causality analysis framework combining high dimensionality independent component analysis (ICA), Granger causality, and least absolute shrinkage and selection operator regression on longitudinal brain metabolic activity data measured by Fluorodeoxyglucose positron emission tomography (FDG-PET). We analyzed FDG-PET images from healthy old subjects, who were scanned for at least five sessions with an averaged intersession interval of 1 year. The longitudinal data were concatenated across subjects to form a time series, and the first-order autoregressive model was used to measure interregional causality among the independent sources of metabolic activity identified using ICA. Several independent sources with reduced metabolic activity in aging, including the anterior temporal lobe and orbital frontal cortex, demonstrated causal influences over many widespread brain regions. On the other hand, the influenced regions were more distributed, and had smaller age-related declines or even relatively increased metabolic activity. The current data demonstrated interregional spreads of aging on metabolic activity at the scale of a year, and have identified key brain regions in the aging process that have strong influences over other regions.

## KEYWORDS

aging, anterior temporal lobe, Granger causality, LASSO regression, metabolic connectivity, orbitofrontal cortex

Data used in preparation of this article were obtained from the Alzheimer's Disease Neuroimaging Initiative (ADNI) database ([adni.loni.usc.edu](http://adni.loni.usc.edu)). As such, the investigators within the ADNI contributed to the design and implementation of ADNI and/or provided data but did not participate in analysis or writing of this report. A complete listing of ADNI investigators can be found at [http://adni.loni.usc.edu/wp-content/uploads/how\\_to\\_apply/ADNI\\_Acknowledgement\\_List.pdf](http://adni.loni.usc.edu/wp-content/uploads/how_to_apply/ADNI_Acknowledgement_List.pdf).

## 1 | INTRODUCTION

The human brain undergoes development and aging across the entire life span. Neuroimaging studies have demonstrated that different brain regions develop and age in different rates. The global gray matter volume decreases linearly after 20 years of age, but some regions such as the bilateral insula, superior parietal gyri, central sulci, and cingulate sulci show faster volumetric declines as measured by voxel-based morphometry (Good et al., 2001). Cortical thickness measures show more widespread cortical thinning patterns during aging (Salat et al., 2004). In contrast, results from functional magnetic resonance imaging (fMRI) studies are more complex with some brain regions show increased activations in certain tasks rather than declined activations accompanied with the anatomical declines (Di, Rypma, & Biswal, 2014; Spreng, Wojtowicz, & Grady, 2010). In addition, the functional alterations in aging may depend on the task domains and behavioral performances (Spreng et al., 2010), making it difficult to conclude a region to be functionally increased or decreased in aging. A complementary approach is to study brain activity during a state without specific behavioral involvements, that is, resting-state. Studies have been performed earlier using positron emission tomography (PET) (Kuhl, Metter, Riege, & Phelps, 1982; Martin, Friston, Colebatch, & Frackowiak, 1991; Zuendorf, Kerrouche, Herholz, & Baron, 2003), and later using resting-state fMRI (Biswal et al., 2010). Using a large sample of over 1,000 subjects, Biswal et al. (2010) have shown reduced resting-state activity in aging mainly in the default model network and increased activity in the visual, motor, and subcortical regions.

Functionally related brain regions typically show similar codevelopments (Alexander-Bloch, Raznahan, Bullmore, & Giedd, 2013) or codeclines, therefore yielding cross-subject interregional covariances. This has been shown as early as 1980s using regional cerebral blood flow data (Prohovnik, Håkansson, & Risberg, 1980) and regional metabolic activity data (Horwitz, Duara, & Rapoport, 1984; Metter, Riege, Kuhl, & Phelps, 1984) measured using PET. Later, more sophisticated methods, such as independent component analysis (ICA) and graph theory-based analysis, have been applied to PET data to study the brain metabolic covariance networks (Di et al., 2017; Di, & Biswal, & Alzheimer's Disease Neuroimaging Initiative, 2012). Correlated metabolic activity or blood flow was typically found between left/right homotopic regions, and between some within hemisphere regions that are functionally related, for example, language-related regions in the left hemisphere. However, different connectivity patterns have been found between this metabolic covariance connectivity and the resting-state connectivity that has been typically observed from fMRI data (Di et al., 2017; Di et al., 2012). The intersubject covariance patterns have also been shown using other imaging modalities, such as brain volumes (Di & Biswal, 2016; Douaud et al., 2014; Mechelli, Friston, Frackowiak, & Price, 2005), cortical thickness (Lerch et al., 2006), and different resting-state fMRI indices (Taylor, Gohel, Di, Walter, & Biswal, 2012; Zhang et al., 2011).

Given the different rates of declines or relative preservations of different brain regions in aging, and large-scale brain networks working in

synchrony during both task execution and resting-state (Bullmore & Sporns, 2009, 2012; Di, Gohel, Kim, & Biswal, 2013), it is likely that the regions that are working together affect each other during the aging process. Specifically, a region that declines faster may influence another region during functional interactions in everyday basis; therefore would cause the other region to decline or show a compensatory increase of functional activity. So, it is critical to study the causal interregional influences between regions rather than the simple covariance, especially at the time scale of months to years when brain aging could be observed. Although regional brain aging is generally assumed to be linear in trend, the observed regional brain measures might showed fluctuations along the linear trend (Figure 1). The causal influence between regions could then be captured by causality analysis methods such as Granger causality (Granger, 1969). By using Granger causality, we could examine whether the brain activity in a brain region at time points of months or years earlier can predict the activity of another brain region at the current time point. Granger causality at the similar time scales has been studied on brain morphological progressions in epilepsy (Zhang et al., 2017) and schizophrenia (Jiang et al., 2018) based on anatomical MRI data. However, both of these studies are cross sectional. Large-scale multisite longitudinal open access dataset, such as Alzheimer's Disease Neuroimaging Initiative (ADNI), has made it possible to examine causal influences during aging in a within-subject manner. Extending our previous work on metabolic covariance networks using Fluodeoxyglucose (FDG) PET images (Di et al., 2017; Di et al., 2012), we sought in the current study to examine the interregional causal influences of metabolic activity during aging.

The aim of the current study is to explore the causal interregional influences of metabolic activity during normal aging at the time scale of a year. We leveraged the longitudinal FDG-PET data from the ADNI dataset, where there were at least five sessions of FDG-PET scans for each subject at a time step of approximately 1 year. First, we examined regional age effects of metabolic activity to identify regions with accelerated declines, with no apparent age effects, and with relative

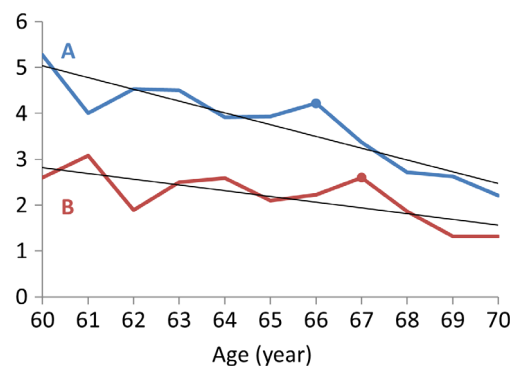


**FIGURE 1** An illustration of interregional causal effects during aging. Regions A and B both show linear declines during aging at different rates, with additional fluctuations along the linear trends. The fluctuations of Region A influences those in Region B, so that an event in A can be observed one time point later in B (e.g., the marked peak at age 66 and 67 in Regions A and B, respectively) [Color figure can be viewed at [wileyonlinelibrary.com](http://wileyonlinelibrary.com)]

increases. Second, we performed whole brain Granger causality analysis to identify causal influences, where the metabolic activity in a region at a certain time point can be predicted by the metabolic activity in another region at the previous time point. We predict that the regions that show accelerated declines during aging will cause other regions to decline, thus showing interregional spreads of age effects.

## 2 | METHODS

### 2.1 | ADNI data

Data used in the preparation of this article were obtained from the ADNI database (ADNI: RRID:SCR\_003007;adni.loni.usc.edu). The ADNI was launched in 2003 as a public-private partnership, led by Principal Investigator Michael W. Weiner, MD. The primary goal of ADNI has been to test whether serial MRI, PET, other biological markers, and clinical and neuropsychological assessment can be combined to measure the progression of mild cognitive impairment (MCI) and early Alzheimer's disease.

Only data from healthy participants were included in the current analysis. All participants showed no signs of depression, MCI, or dementia, with Mini-Mental State Exam scores between 24 and 30 and Clinical Dementia Rating score of 0. We manually selected longitudinal FDG-PET images from the ADNI database, with participants who had at least five sessions of FDG-PET images available. As a result, 72 subjects (25 females) were included in the current analysis with a total of 432 PET scan sessions. The numbers of available sessions ranged from 5 to 9 (Figure 2a). The average age at the first session was 75.8 years (62–86 years). For each session, we calculated a mean image or adopted the only image to represent the session. The intersession interval with a subject varied from 3 months to up to 8 years for a few rare cases (Figure 2b). The mean and median of the intersession intervals were 1.02 and 0.98 years, respectively.

The FDG-PET images were acquired from multiple sites with different PET imaging protocols. However, the imaging parameters were mostly similar across different sessions within a subject. Since the current analyses were all within-subject, the impacts of different imaging parameters from different sites can be effectively minimized. More

information about the PET protocol can be found in (Jagust et al., 2010). All the images and subjects included in the current analysis can be found at <https://osf.io/4a3vt/>.

### 2.2 | PET data preprocessing

The PET data were preprocessed using SPM12 (SPM: RRID:SCR\_007037; <https://www.fil.ion.ucl.ac.uk/spm/>) under MATLAB R2017b. For each subject, if there were more than one PET image in a session, all the PET images in the session were realigned to the first image and the mean image of the session was calculated. The mean images (or the only image) across all the sessions of a subject were then realigned to the one in the first session. The cross-session mean image was normalized directly to the PET template in SPM in standard Montreal Neurological Institute (MNI) space, and then all the images were normalized to MNI space using the same set of parameters. We chose the direct normalization approach rather than using an anatomical MRI as a mediator, because the spatial resolutions of the PET images were adequate and the direct normalization has its own advantage compared with the anatomical MRI-mediated method (Calhoun et al., 2017). The images were then spatially smoothed using a Gaussian kernel with 8 mm full width at half maximum. Finally, each image was divided by its mean signal within an intracranial volume mask.

### 2.3 | Independent component analysis

We first performed spatial ICA to separate the whole brain metabolic maps into independent sources of local metabolic variations (Di, & Biswal, and Alzheimer's Disease Neuroimaging Initiative, 2012). We extracted a relatively high number of ICs, so that the resulting ICs could represent more local variations than large-scale networks (Fu et al., 2018, 2019; Smith et al., 2013). This data-driven approach is an alternative to atlas-based parcellation, and may be more representative to local variations of metabolic activity. The ICA was performed using Group ICA of fMRI Toolbox (GIFT: RRID:SCR\_001953; <http://mialab.mrn.org/software/gift>) (Calhoun, Adali, Pearlson, & Pekar, 2001). The preprocessed FDG-PET images from different sessions and subjects were concatenated into a single time series, and fed into

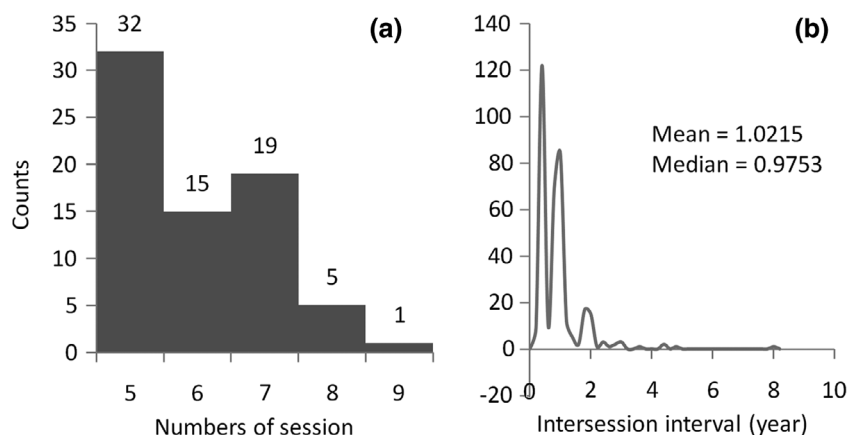


**FIGURE 2** Histograms of the numbers of sessions for each subject (a) and the intersession intervals for all the sessions and subjects (b). The participants were typically studied at 0, 6, 12, 24, and 36 months related to the first visit, and yearly follow-ups. Therefore, the intersession intervals are likely to be around 6 months or 1 year

the ICA analysis. Eighty-one components were recommended by the minimum description length algorithm implemented in GIFT. After extraction of the 81 components, the ICs were visually inspected and grouped into eight domains (Supporting Information) as well as 21 noise components. There were in total 60 ICs included in the following analysis. For each IC, the associated time series were obtained to represent metabolic activity of this source in different subjects and sessions. The 81 IC maps are available at <https://osf.io/4a3vt/>.

## 2.4 | Regional age effects

For each subject, a general linear model (GLM) was built to examine aging effects. The GLM included two regressors, a constant term and a linear age effect. The GLM analysis was performed on each IC, and the  $\beta$  values of the age effect were obtained. Group level analysis was then performed on each IC using a one sample *t*-test model to examine the group averaged effect of age. A false discovery rate (FDR) corrected  $p < .05$  was used to identify ICs that had significant age effects after correcting for all the 60 comparisons. Thereafter, the ICs were sorted into three groups, with significant (relative) increased metabolic activity, with no significant changes, and with significant decreased metabolic activity in aging.

## 2.5 | Interregional causality analysis

We adopted Granger causality to examine the interregional causal influence of metabolic activity. Specifically, we treated the longitudinal FDG-PET data as time series, and used autoregressive model to predict the value of time point *t* in a region *y* by the previous time points of another region *x*, when controlling for its own previous time points. In the current data, the time step is approximately 1 year. To account for the variability of intersession interval, the intervals between time points *t* and *t*−1 were added as a covariate or regressed out in the analysis (see below for details). Another consideration is the order of the model, that is, how many previous time points are used to predict the current time point. In this study, we used only the first order model to measure the causal influence of only one previous time point, which represents a time step of about 1 year. The limited number of time points in a subject prevents us to use higher order models. The advantage of using only the first order model is that the sign information of the beta estimate enables us to differentiate positive and negative predictions. The model can be expressed in the following form:

$$y_t = \beta_0 + \beta_1 \cdot y_{t-1} + \beta_2 \cdot x_{t-1} + \varepsilon$$

where *y* represents the predicted time series in one brain region, and *x* represents the predicting time series of another brain region.  $y_{t-1}$  represents the time series of  $y_t$  which moved one time point ahead, thus representing a autoregression model of time series *y*. The effect of interest is the predicting value of  $x_{t-1}$ , which is  $\beta_2$ .

We concatenated the time series across all the subjects to form a long time series for analysis (Figure 3). Therefore, the model is considered fixed effect model. The time series of a subject were first *z*

transformed to minimize intersubject variation, where  $m_i$  represents the total number of time points in a subject *i*. For each subject, we included the time points 2 to *m* of the time series of a region as the predicted variable  $y_t$ . The autoregressive variable  $y_{t-1}$  included the time points 1 to *m*−1 of the time series of the same region. The predicting variable  $x_{t-1}$  was the time points 1 to *m*−1 from another region *x*. After concatenation, there were in total 360 data points in the time series.

The model could be applied to each pair of the ICs from the 60 ICs. The intersession interval between time *t* and time *t*−1 were included in the model as a covariate. We first performed such analysis on each pair of ICs to obtain the predicting effect ( $\beta_2$ ) and corresponding *p* values, which formed a 60 × 60 matrix of causal effects. FDR correction at  $p < .05$  was used to correct for multiple comparisons of the in total 3,540 (60 × 59) effects, where the autoregressive effects along the diagonal were not tested.

This pairwise approach may identify influences from different regions with shared variance although maybe only one region has direct influence with the tested region. To overcome this, when predicting a region  $x_t^i$ , one can add all the other ICs to identify which region can predict  $x_t^i$ . The model is then as following for a predicted region  $x_t^i$ :

$$x_t^i = \beta_0 + \beta_1 \cdot x_{t-1}^1 + \beta_2 \cdot x_{t-1}^2 + \beta_3 \cdot x_{t-1}^3 + \dots + \beta_p \cdot x_{t-1}^p + \varepsilon$$

Since all the ICs were included in the model, there was no need to differentiate the variables of *x* and *y*. Therefore, we use *x* to denote all the time series variables. The superscripts of *x* now represent different ICs, where *p* represents the total number of the ICs. Before entering in to the model, a time series representing the intersession interval between time point *t* and *t*−1 were regressed out from all the  $x_{t-1}$  time series to account for the intersession interval variability. Estimating the multivariate model may be challenging, especially when some of the IC time series may be highly correlated. It can be assumed that only a small number of ICs may influence the predicted IC. In this scenario, one can use regularization method to estimate the sparse influence effects, such as using least absolute shrinkage and selection operator (LASSO) (Tang, Bressler, Sylvester, Shulman, & Corbetta, 2012; Tibshirani, 1996). The motivation of choosing LASSO over other regularization methods is that the LASSO regularization can force some parameters in the model to be zero thus resulting in only a small number of nonzero parameters. This is important in the current context, because the aim is to identify a small number of interregional influences. Since this model examines the prediction of the time series of one IC by the time series of all the other ICs, the analysis only needed to be performed for 60 times (compared with 60 × 59 times in the pairwise analysis) to cover all the interregional influences.

The LASSO regression was performed using the lasso function implemented in MATLAB. To determine an optimal regularization factor  $\lambda$ , we used a set of  $\lambda$  from 0 (no regularization) to 0.5 with a step of 0.001. The identified nonzero influences dropped dramatically as the increase of  $\lambda$ . We identify the  $\lambda$  where the number of nonzero influences were the closest to the number of significant effects when using FDR correction in the pairwise analysis, and reported all the nonzero influencing effects.

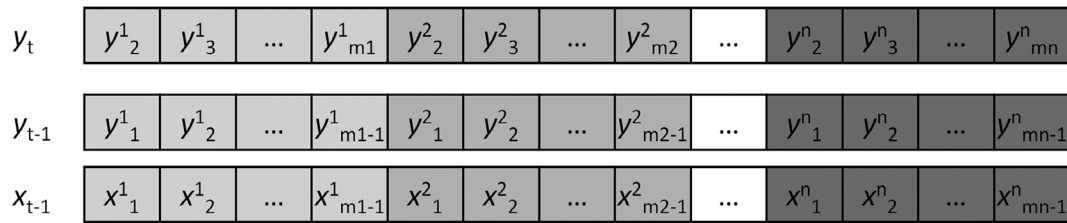


**FIGURE 3** Illustration of the construction of the variables used in the causality analysis.  $x$  represents the predicting region, and  $y$  represents the predicted region. The superscript represents different subjects, with a total number of  $n$ . The subscript represents the scan session in a subject, with a total number of  $m_i$  for a subject  $i$

The resulting  $60 \times 60$  influencing matrix can be treated as a directed network graph, where the ICs represent the nodes and the causal influences represent directed edges of the graph. We calculated in-degree and out-degree of the 60 nodes to characterize the importance of an IC in the whole brain influencing graph. To ensure that the degree calculation was not affected by arbitrary defined threshold, we also explored the graphs from other  $\lambda$  values to verify the identified hub regions are still present. To visualize the network topology, we identified the giant component where all the nodes in the component were somehow connected (without considering the direction of the influences). The giant components were visualized using the force layout.

### 3 | RESULTS

#### 3.1 | Age effect on regional metabolic activity

We first examined the age effects on the regional metabolic activity for the 60 ICs. Statistical significant ICs at  $p < .05$  after FDR correction are shown in Figure 4. Eighteen ICs showed significant reduced metabolic activity, including one IC that covered the inferior portion of the cerebellum (IC 1), three ICs that covered visual cortex (IC 17, 32, and 53), three ICs that covered the posterior parietal cortex (IC 21, 27, and 28), five ICs that covered the anterior portion of the temporal lobe and insula (IC 24, 44, 63, 66, and 77), one IC that covered the thalamus and basal ganglia (IC 23), two ICs that covered the orbital frontal cortex and frontal pole (IC 3 and 48), and three ICs that covered the cingulate cortex and neighboring midline cortical regions (IC 7, 37, and 46). The left panel of Figure 5 illustrates the negative age effects of an example IC (IC 48). It can be seen that there is a general linear trend of decrease of metabolic activity. However, each subject showed fluctuations of metabolic activity along the linear trend. In contrast, six ICs showed increased metabolic activity. It should be noted that due to the nature of PET imaging, the global signal for each PET image has to be normalized. Therefore, it is difficult to say whether the positive age effect represents increased metabolic activity, or a relative increase with reference to the global effect. The ICs with relative increased metabolic activity during aging included one IC covering the inferior and posterior portion of the cerebellum (IC 13), two subcortical ICs covering the basal ganglia, insula, amygdala, and thalamus (IC 19 and 52), and three ICs of sensorimotor regions (IC 36,

50, and 68). The right panel of Figure 5 illustrates the positive age effects of an example IC (IC 19). There were 36 ICs that did not show statistically significant age effects at  $p < .05$  after FDR correction. The middle panel of Figure 5 illustrates the age effects of an example IC (IC 56) with no statistical significant age effect.

#### 3.2 | Interregional causal influences of metabolic activity

We first applied pairwise autoregressive model to obtain a  $60 \times 60$  matrix of the interregional causal influences of metabolic activity between each pair of the ICs (Figure 6a). When using a statistical threshold of  $p < .05$  of FDR correction, 14 positive and 13 negative causal influences were identified (Figure 6b). We next performed LASSO regression with  $x_t$  of an IC as the predicted variable and  $x_{t-1}$  of all the ICs as the predicting variables using a range of  $\lambda$ . We identified the  $\lambda$  value where the number of nonzero effects was the closest to the number of significant effects in the pairwise analysis. The resulting influencing effects at  $\lambda = 0.162$  (Figure 6c) look in general similar to the significant effects identified by the pairwise analysis, although some subtle differences can be noted. There were 15 positive and 13 negative causal influences identified using LASSO regression (Table 1).

Among the 28 causal influences from LASSO regression, the first giant component was comprised of 26 causal influences involving 25 ICs (Figure 7). The IC maps were color-coded based on their regional age effects to illustrate the relationships between regional metabolic activity changes and the signs of causal influences. It can be seen that the influences between two decreased regions or two increased regions in aging were in general positive, but the influences between one increased and one decreased regions were in general negative. For example, the bilateral anterior temporal IC (IC 63 in Figure 6) positively influenced the medial parietal IC (IC 27), but negatively influenced the basal ganglia IC (IC 19). It is consistent with the direction of the spread of age effects. There were also ICs that without apparent age effects, where the signs of causal influences with other regions did not show clear pattern.

To better illustrate the topology of the interregional influencing network and to highlight the regions that are more influencing or influenced to other regions, we plotted the first giant components of the interregional influencing network using force layout at  $\lambda = 0.162$ ,

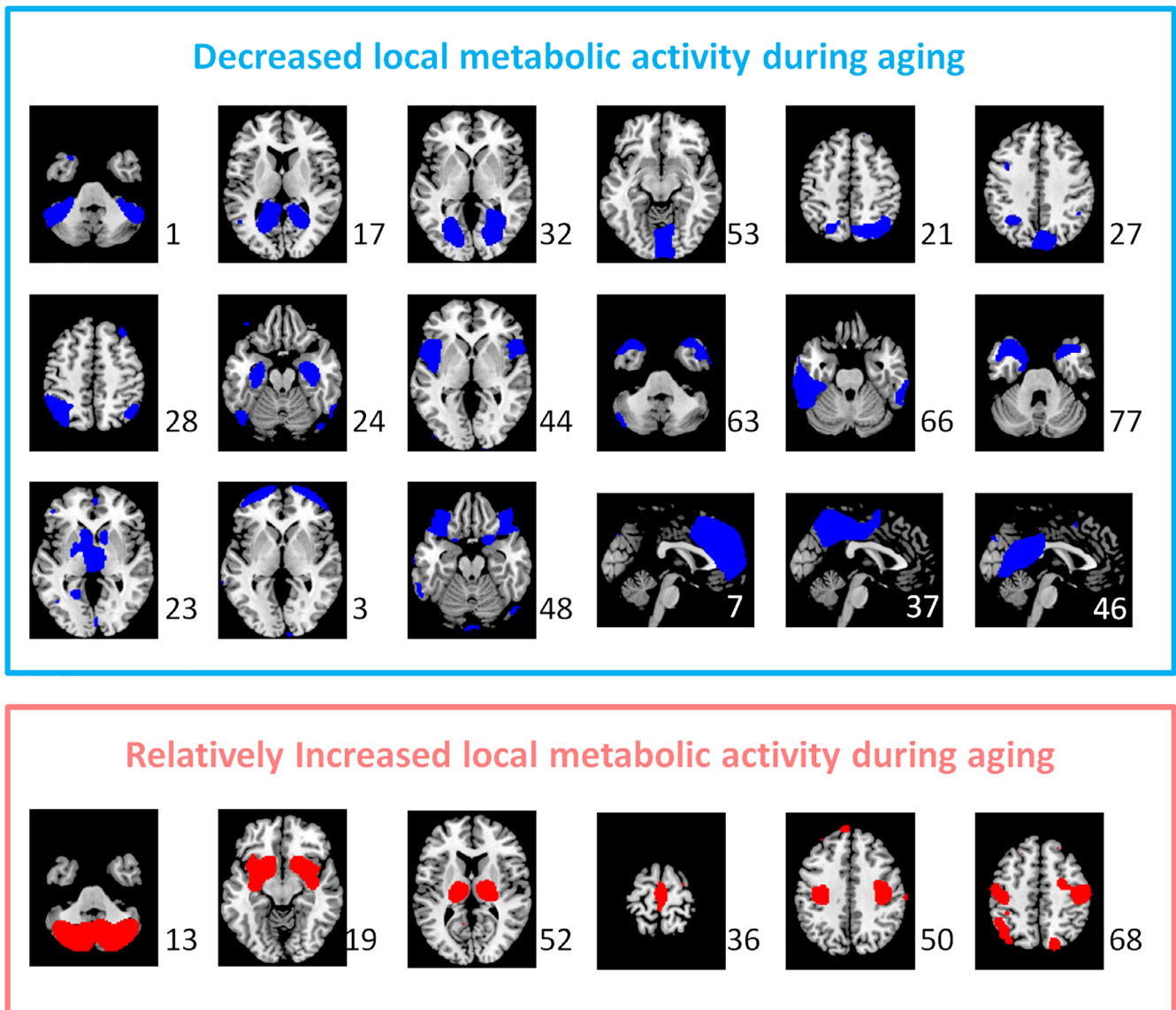


**FIGURE 4** The independent components (ICs) that showed statistically significant decreased (blue) and increased (red) metabolic activity during aging after controlling for global effect at  $p < .05$  with false discovery rate (FDR) correction. The numbers to the bottom right represent the IC number [Color figure can be viewed at [wileyonlinelibrary.com](http://wileyonlinelibrary.com)]

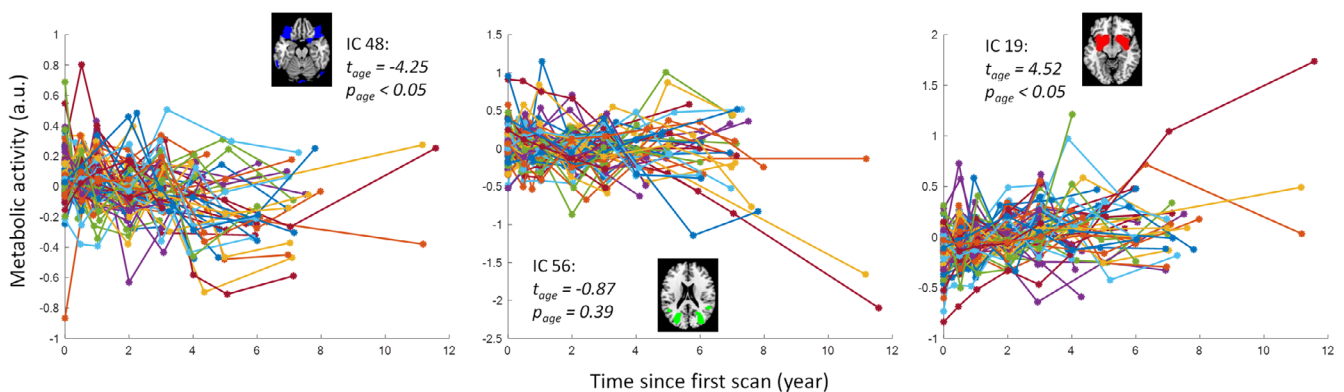


**FIGURE 5** Examples of aging effects of metabolic activity of three independent components (ICs) that had negative, nonsignificant, and positive aging effects. Each colored line represents one subject.  $t$  and  $p$  values represent group-level one sample  $t$ -test statistics. A.u., arbitrary unit [Color figure can be viewed at [wileyonlinelibrary.com](http://wileyonlinelibrary.com)]

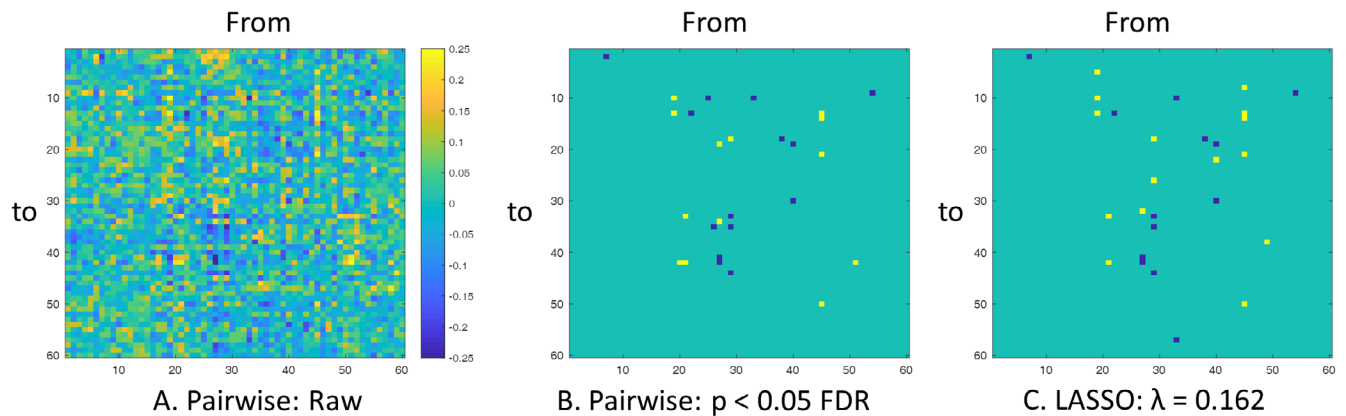


**FIGURE 6** (a) Pairwise matrix of interregional causal influence of metabolic activity. The columns represent influencing independent components (ICs), while the rows represent influenced ICs. (b) Ternary matrix of significant positive or negative interregional causal influences thresholded at  $p < .05$  after false discovery rate (FDR) correction. (c) Ternary matrix of positive or negative interregional causal influences identified at  $\lambda = 0.162$  using least absolute shrinkage and selection operator (LASSO) regression [Color figure can be viewed at [wileyonlinelibrary.com](http://wileyonlinelibrary.com)]

and also at more liberal thresholds of  $\lambda = 0.142$  and  $\lambda = 0.122$  (Figure 8). The node sizes represent the out-degree and in-degree of a node in the network in the upper and middle panels, respectively. It can be seen that the nodes with large out-degree were in general the regions with decreased metabolic activity (blue nodes). The red arrows highlighted the two nodes that had five out-degrees at  $\lambda = 0.162$  and remained among the highest out-degree nodes at the lower  $\lambda$  values. These two nodes were also highlighted in Figure 7, which covered the bilateral orbitofrontal cortex (IC 48) and the bilateral anterior temporal lobe (IC 63). While in terms of in-degree, there were no clear regions that had exceptionally high in-degree compared with other nodes. The node with high in-degree had no apparent age effects (green nodes) or had increased metabolic activity with age (brown nodes). The distributions of nodal out- and in-degree confirmed that the out-degree distributions had heavy tailed distributions compared with the in-degree distributions (lower panels in Figure 8).

## 4 | DISCUSSION

By applying autoregressive model on longitudinal FDG-PET data, the current study demonstrated causal interregional influences of metabolic activity during normal aging. Several ICs with significant reduced metabolic activity in aging, including the orbital frontal cortex and anterior temporal lobe, causally influenced many other ICs. In contrast, the influenced ICs were more widespread and with less local aging effects or even with relatively increased metabolic activity. To the best of our knowledge, this is the first study to demonstrate longitudinal interregional causal influences of brain activity during aging at the time scale of a year.

Consistent with our predictions of interregional spreads of age effects, the influencing ICs usually had decreased metabolic activity. On the other hand, the influenced regions were not restricted to the regions with reduced metabolic activity in aging. Indeed, the ICs that had relatively greater in-degree values than other ICs were usually

without apparent age effects, or even with relatively increased metabolic activity, for example, the basal ganglia and thalamus. Therefore, the causal interregional influences in general reflected the spread of age effects from brain regions that had already declined to regions that are declining or relatively preserved. We note that the absence of regional age effects should be interpreted with caution, because the removal of global effects during calculation of regional age effects could have removed significant age effects that were similar to the global effects.

The interpretation of the causal influences need to consider both the sign of the causal influences and the regional age effects. A positive influence indicates that the metabolic activity in Region A at the current time point positively predicts the metabolic activity in Region B at the next time point. While a negative influence indicates a negative prediction. If the two regions are both decreasing during aging, then a positive influence may indicate a spread of metabolic activity decline between the two regions. On the other hand, if Region A decreases but Region B shows relatively increased metabolic activity, and there is a negative influence between A and B, then it may indicate a compensation of Region B that is resulted from the declined function of Region A. A close look at the patterns of the directions of the local and interregional effects indicated that most of the effects observed were consistent with the spatial spread or compensation interpretations. That is, the influences between two decreased regions were all positive, and the influences between one decreased region and one increased regions were all negative.

The current analysis identified several hubs that influenced other brain regions, most prominently the anterior temporal lobe and orbital frontal cortex. The anterior temporal lobe (IC 63) is connected to several major white matter tracts such the cingulum, inferior longitudinal fasciculus, and uncinate fasciculus (Catani & Thiebaut de Schotten, 2008), which could support its influencing role to other regions such as the subcortical regions, inferior frontal cortex, and left temporal cortex. To better characterize its functional correlates, we submitted

**TABLE 1** List of interregional causal influences of metabolic activity identified at  $\lambda = 0.162$  using LASSO regression

From		→ Sign	To	
IC #	Label		IC #	Label
52	Thalamus, brainstem	–	27	Precuneus
36	Supplementary motor area, paracentral lobule	+	52	Thalamus, brainstem
44	Insula, inferior frontal gyrus, superior temporal pole	+	77	Temporal pole, medial orbitofrontal cortex
63	Temporal pole	+	40	Left middle temporal gyrus
63	Temporal pole	+	27	Precuneus
44	Insula, inferior frontal gyrus, superior temporal pole	–	20	Right inferior and middle frontal gyrus
63	Temporal pole	–	38	Left thalamus, caudate, lingual gyrus
44	Insula, inferior frontal gyrus, superior temporal pole	–	16	Superior and middle frontal gyrus
39	Superior parietal lobule, precuneus	+	20	Right inferior and middle frontal gyrus
19	Basal ganglia, amygdala, insula	–	46	Posterior cingulate cortex, precuneus, lingual gyrus
63	Temporal pole	–	19	Basal ganglia, amygdala, insula
63	Temporal pole	–	34	Inferior frontal gyrus
81	Lobule VII crus, lobule VI hemisphere, vermis	–	6	Lobule VII crus
39	Superior parietal lobule, precuneus	+	19	Basal ganglia, amygdala, insula
19	Basal ganglia, amygdala, insula	–	17	Lingual gyrus, calcarine sulcus, cuneus
48	Orbitofrontal cortex, superior temporal pole	+	39	Superior parietal lobule, precuneus
28	Inferior parietal lobule, precuneus	+	17	Lingual gyrus, calcarine sulcus, cuneus
48	Orbitofrontal cortex, superior temporal pole	+	47	Postcentral gyrus, inferior parietal lobule
48	Orbitofrontal cortex, superior temporal pole	+	56	Superior and middle occipital gyrus
28	Inferior parietal lobule, precuneus	+	56	Superior and middle occipital gyrus
28	Inferior parietal lobule, precuneus	+	43	Lobule VII and VIII, hemisphere
48	Orbitofrontal cortex, superior temporal pole	+	11	Lingual gyrus, calcarine sulcus, cuneus
48	Orbitofrontal cortex, superior temporal pole	+	69	Inferior occipital and fusiform gyrus
80	Inferior parietal lobule	–	56	Superior and middle occipital gyrus
5	Left inferior frontal gyrus, left middle occipital gyrus	–	28	Inferior parietal lobule, precuneus
78	Postcentral gyrus	–	12	Superior and middle occipital gyrus
5	Left inferior frontal gyrus, left middle occipital gyrus	+	80	Inferior parietal lobule
5	Left inferior frontal gyrus, left middle occipital gyrus	–	66	Left inferior temporal gyrus

Abbreviation: LASSO, least absolute shrinkage and selection operator.

the IC map into NeuroVault (NeuroVault, RRID:SCR\_003806; <https://neurovault.org>), and decoded the functions of these maps using large-scale meta-analytic data from NeuroSynth (NeuroSynth, RRID:SCR\_006798; <http://neurosynth.org/>) (Rubin et al., 2017). The first five functional terms were all about language and semantic processing (see Table S2, Supporting Information). Studies also showed that electrical stimulation of the anterior temporal lobe can improve proper name recalls in aging (Ross, McCoy, Coslett, Olson, & Wolk, 2011), and bilingualism can protect the integrity of anterior temporal lobe in aging (Abutalebi et al., 2014). Taken together, the results suggest that language process might be an important factor modulating brain aging.

The orbital frontal cortex (IC 48) is connected to the uncinatus fasciculus and inferior fronto-occipital fasciculus (Catani & Thiebaut de Schotten, 2008), which could support its influences to the posterior visual regions. The functional words related to the orbitofrontal IC were mainly about emotional processing (Table S2, Supporting Information). In older

population, smaller orbitofrontal volumes are shown to be associated with depression (Lai, Payne, Byrum, Steffens, & Krishnan, 2000; Taylor et al., 2003). Taken together, emotional process might also be an important factor modulating brain aging. However, although previous studies have shown associations between resting-state brain activity and task activations (Di, Kannurpatti, Rypma, & Biswal, 2013; Yuan et al., 2013), the extent to what resting-state brain activity can reflect certain brain functions are still largely unknown. Further studies might need to design proper tasks to better link functions to brain activations.

A limitation of the current analysis is the potential confounding effect due to partial volume (Bonte et al., 2017; Rousset, Ma, & Evans, 1998), that is, whether an observed effect is due to the changes of bona fide metabolic activity or the changes of underlying gray matter volume. However, the following reasons make the partial volume confounding less problematic. First, the current analysis adopted within subject comparison, which has already minimized the partial volume



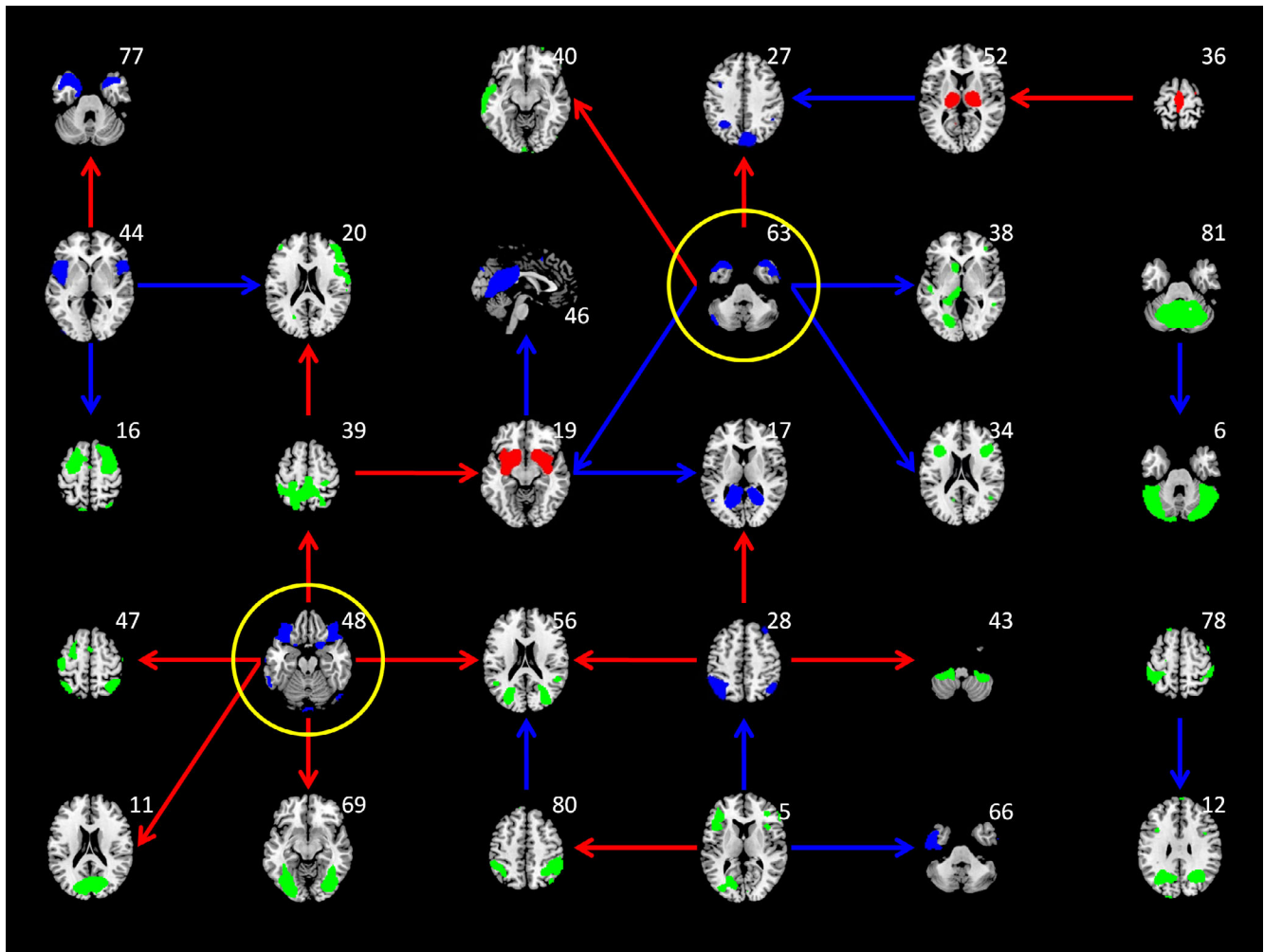


**FIGURE 7** Interregional causal influences network at  $\lambda$  of 0.162 using least absolute shrinkage and selection operator (LASSO) regression. The colors of the independent component maps represent increased (red), decreased (blue), and nonsignificant (green) age effects on metabolic activity. The colors of the arrows represent positive (red) and negative (blue) interregional influences, respectively. The maps highlighted with yellow circle represent hub regions in the network [Color figure can be viewed at [wileyonlinelibrary.com](http://wileyonlinelibrary.com)]

effects due to inter subject anatomical variability. Second, we applied ICA to identify independent sources of metabolic variability. Some components that were likely due to enlargement of ventricle and are spatially overlapped with the included ICs, have been already removed. For example, there was an IC largely located in ventricle area (IC 79 in Figure S9, Supporting Information) but with substantial overlaps with the ICs of the thalamus and basal ganglia (Figure S5, Supporting Information). The IC 79 had the second strongest negative age effect among all the ICs. The included ICs that had spatial overlap with this IC showed no age effects or even positive age effects, suggesting that the partial volume effects associated with enlarged ventricle have been minimized in these ICs. Third, even though the observed causal influences may still somehow contributed by the residual partial volume effects, the causal influences of volumetric reductions may still be important findings for understanding brain aging. The structural MRI images are available in the ADNI dataset, but were not always acquired at the same time point as the PET images, making the incorporation of MRI images in the model difficult.

Future studies should certainly consider taking into account of anatomical information in the analysis. Indeed, it may be theoretically more important to study the interaction or causal influences between brain anatomy and functions in aging. According to the compensation model, the reduction of gray matter will lead to elevated functional responses, which then give rise to less affected behavioral performances (Gregory et al., 2018; Reuter-Lorenz & Park, 2014; Shafto & Tyler, 2014). A direct examination of causal influences among local and interregional gray matter structures, functions, and behavioral performances may provide more insight to the dynamic of compensation process in aging.

One strength of the current analysis approach is that we adopted multivariate methods and LASSO to include all the ICs in the predicting models, which in theory can prevent identifying ICs that have indirect predicting effects to the target (Smith et al., 2011; Tang et al., 2012). On the other hand, there are also several simplifications of the Granger causality analysis, such as the inclusion of only the first order model and the assumption of equal time steps. Since the current study is the first to explore the causality in the aging process, the time

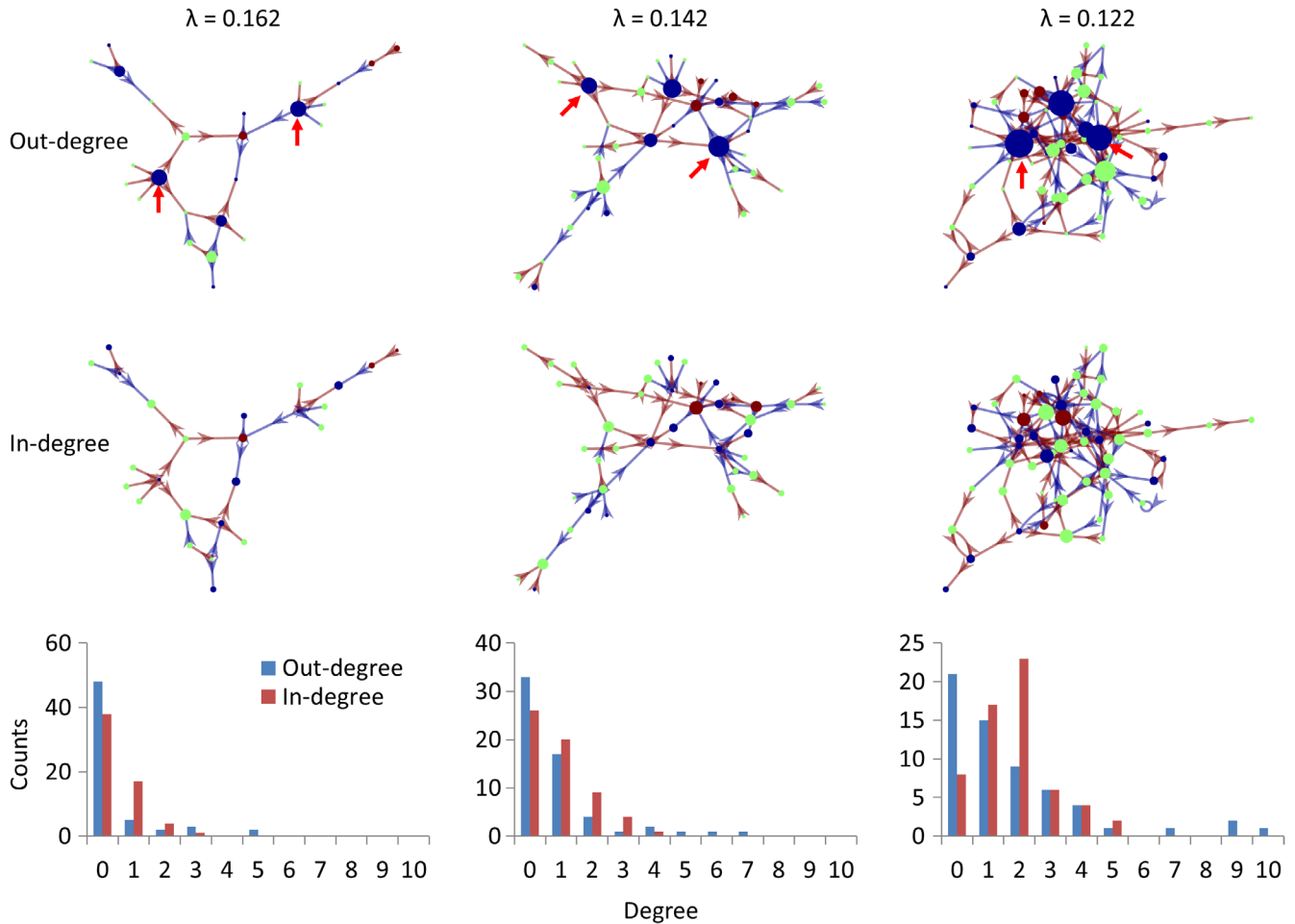


**FIGURE 8** The giant component of the causal interregional influencing network of metabolic activity at different  $\lambda$  levels with the sizes of the nodes reflecting out-degree (top row) and in-degree (middle row). The bottom row shows the degree distributions of the whole influencing network at the three  $\lambda$  levels. Brown and blue arrows indicate positive and negative influences identified using least absolute shrinkage and selection operator (LASSO) regression. Blue, green, and brown regions indicate positive, none, and negative age effects on regional metabolic activity. The red arrows highlight the two influencing nodes at different  $\lambda$  levels [Color figure can be viewed at [wileyonlinelibrary.com](http://wileyonlinelibrary.com)]

lag of the aging progression is still largely unknown and bear further studies. However, practically due to the limited availability of longitudinal data, this question is difficult to solve at the current stage. Regarding the variable time steps of the time series, we added the intersession interval as a covariate to minimize the effects, which is similar to a previous work (Jiang et al., 2018). More sophisticated models, such as generative model and differential equation-based method (Ziegler, Penny, Ridgway, Ourselin, & Friston, 2015; Gabriel Ziegler, Ridgway, Blakemore, Ashburner, & Penny, 2017), may be used in future to better characterize the causal effects.

## 5 | CONCLUSION

By applying Granger causality analysis on longitudinal FDG-PET images of healthy old participants at a time step of 1 year, the current analysis revealed interregional causal influences during aging. Several regions with reductions in local metabolic activity during aging, including the bilateral anterior temporal lobe and orbitofrontal cortex,

showed causal influences to other regions, supporting an interregional spread of age effects in the brain. The current analysis and results could add new insights to the neurocognitive aging literature about interregional interactions during the aging process.

## ACKNOWLEDGMENTS

The theoretical work and data analysis were funded by (U.S.) National Institute of Health grants: R01AT009829 and R01DA038895. Data collection and sharing for this project was funded by the Alzheimer's Disease Neuroimaging Initiative (ADNI) (National Institutes of Health Grant U01 AG024904) and DOD ADNI (Department of Defense award number W81XWH-12-2-0012). ADNI is funded by the National Institute on Aging, the National Institute of Biomedical Imaging and Bioengineering, and through generous contributions from the following: AbbVie, Alzheimer's Association; Alzheimer's Drug Discovery Foundation; Araclon Biotech; BioClinica, Inc.; Biogen; Bristol-Myers Squibb Company; CereSpir, Inc.; Cogstate; Eisai Inc.; Elan Pharmaceuticals, Inc.; Eli Lilly and Company;

EuroImmun; F. Hoffmann-La Roche Ltd and its affiliated company Genentech, Inc.; Fujirebio US; GE Healthcare; IXICO Ltd.; Janssen Alzheimer Immunotherapy Research & Development, LLC.; Johnson & Johnson Pharmaceutical Research & Development, LLC.; Lumosity; Lundbeck; Merck & Co., Inc.; Meso Scale Diagnostics, LLC.; NeuroRx Research; Neurotrack Technologies; Novartis Pharmaceuticals Corporation; Pfizer Inc.; Piramal Imaging; Servier; Takeda Pharmaceutical Company; and Transition Therapeutics. The Canadian Institutes of Health Research is providing funds to support ADNI clinical sites in Canada. Private sector contributions are facilitated by the Foundation for the National Institutes of Health ([www.fnih.org](http://www.fnih.org)). The grantee organization is the Northern California Institute for Research and Education, and the study is coordinated by the Alzheimer's Therapeutic Research Institute at the University of Southern California. ADNI data are disseminated by the Laboratory for Neuro Imaging at the University of Southern California.

## AUTHOR CONTRIBUTIONS

X.D. conceived the idea, and developed and performed the data analysis. All authors discussed the results, and contributed to the final manuscript.

## CONFLICT OF INTEREST

The authors declare that there is no conflict of interest regarding the publication of this article.

## DATA AVAILABILITY STATEMENT

All the data used in this manuscript were from ADNI, an open source database.

## ORCID

Xin Di  <https://orcid.org/0000-0002-2422-9016>

Bharat B. Biswal  <https://orcid.org/0000-0002-3710-3500>

## REFERENCES

- Abutaleb, J., Canini, M., Della Rosa, P. A., Sheung, L. P., Green, D. W., & Weekes, B. S. (2014). Bilingualism protects anterior temporal lobe integrity in aging. *Neurobiology of Aging*, 35(9), 2126–2133. <http://doi.org/10.1016/j.neurobiolaging.2014.03.010>
- Alexander-Bloch, A., Raznahan, A., Bullmore, E., & Giedd, J. (2013). The convergence of maturational change and structural covariance in human cortical networks. *The Journal of Neuroscience*, 33(7), 2889–2899. <http://doi.org/10.1523/JNEUROSCI.3554-12.2013>
- Biswal, B. B., Mennes, M., Zuo, X.-N., Gohel, S., Kelly, C., Smith, S. M., ... Milham, M. P. (2010). Toward discovery science of human brain function. *Proceedings of the National Academy of Sciences of the United States of America*, 107(10), 4734–4739. <http://doi.org/10.1073/pnas.0911855107>
- Bonte, S., Vandemaële, P., Verleden, S., Audenaert, K., Deblaere, K., Goethals, I., & Van Hoen, R. (2017). Healthy brain ageing assessed with 18F-FDG PET and age-dependent recovery factors after partial volume effect correction. *European Journal of Nuclear Medicine and Molecular Imaging*, 44(5), 838–849. <http://doi.org/10.1007/s00259-016-3569-0>
- Bullmore, E., & Sporns, O. (2009). Complex brain networks: Graph theoretical analysis of structural and functional systems. *Nature Reviews Neuroscience*, 10(3), 186–198. <http://doi.org/10.1038/nrn2575>
- Bullmore, E., & Sporns, O. (2012). The economy of brain network organization. *Nature Reviews Neuroscience*, 13(5), 336–349. <http://doi.org/10.1038/nrn3214>
- Calhoun, V. D., Adali, T., Pearlson, G. D., & Pekar, J. J. (2001). A method for making group inferences from functional MRI data using independent component analysis. *Human Brain Mapping*, 14(3), 140–151. Retrieved from <http://www.ncbi.nlm.nih.gov/pubmed/11559959>
- Calhoun, V. D., Wager, T. D., Krishnan, A., Rosch, K. S., Seymour, K. E., Nebel, M. B., ... Kiehl, K. (2017). The impact of T1 versus EPI spatial normalization templates for fMRI data analyses. *Human Brain Mapping*, 38(11), 5331–5342. <http://doi.org/10.1002/hbm.23737>
- Catani, M., & Thiebaut de Schotten, M. (2008). A diffusion tensor imaging tractography atlas for virtual in vivo dissections. *Cortex*, 44(8), 1105–1132. <http://doi.org/10.1016/j.cortex.2008.05.004>
- Di, X., & Biswal, B. B. (2016). Similarly expanded bilateral temporal lobe volumes in female and male children with autism Spectrum disorder. *Biological Psychiatry: Cognitive Neuroscience and Neuroimaging*, 1(2), 178–185. <http://doi.org/10.1016/j.bpsc.2015.11.006>
- Di, X., Biswal, B. B., & Alzheimer's Disease Neuroimaging Initiative. (2012). Metabolic brain covariant networks as revealed by FDG-PET with reference to resting-state fMRI networks. *Brain Connectivity*, 2(5), 275–283. <http://doi.org/10.1089/brain.2012.0086>
- Di, X., Gohel, S., Kim, E. H., & Biswal, B. B. (2013). Task vs. rest-different network configurations between the coactivation and the resting-state brain networks. *Frontiers in Human Neuroscience*, 7, 493. <http://doi.org/10.3389/fnhum.2013.00493>
- Di, X., Gohel, S., Thielcke, A., Wehr, H. F., Biswal, B. B., & Alzheimer's Disease Neuroimaging Initiative. (2017). Do all roads lead to Rome? A comparison of brain networks derived from inter-subject volumetric and metabolic covariance and moment-to-moment hemodynamic correlations in old individuals. *Brain Structure and Function*, 222(8), 3833–3845. <http://doi.org/10.1007/s00429-017-1438-7>
- Di, X., Kannurpatti, S. S., Rypma, B., & Biswal, B. B. (2013). Calibrating BOLD fMRI activations with neurovascular and anatomical constraints. *Cerebral Cortex*, 23(2), 255–263. <http://doi.org/10.1093/cercor/bhs001>
- Di, X., Rypma, B., & Biswal, B. B. (2014). Correspondence of executive function related functional and anatomical alterations in aging brain. *Progress in Neuro-Psychopharmacology & Biological Psychiatry*, 48, 41–50. <http://doi.org/10.1016/j.pnpb.2013.09.001>
- Douaud, G., Groves, A. R., Tamnes, C. K., Westlye, L. T., Duff, E. P., Engvig, A., ... Johansen-Berg, H. (2014). A common brain network links development, aging, and vulnerability to disease. *Proceedings of the National Academy of Sciences of the United States of America*, 111(49), 17648–17653. <http://doi.org/10.1073/pnas.1410378111>
- Fu, Z., Tu, Y., Di, X., Du, Y., Pearlson, G. D., Turner, J. A., ... Calhoun, V. D. (2018). Characterizing dynamic amplitude of low-frequency fluctuation and its relationship with dynamic functional connectivity: An application to schizophrenia. *NeuroImage*, 180, 619–631. <http://doi.org/10.1016/j.neuroimage.2017.09.035>
- Fu, Z., Tu, Y., Di, X., Du, Y., Sui, J., Biswal, B. B., ... Calhoun, V. D. (2019). Transient increased thalamic-sensory connectivity and decreased whole-brain dynamism in autism. *NeuroImage*, 190, 191–204. <http://doi.org/10.1016/j.neuroimage.2018.06.003>
- Good, C. D., Johnsrude, I. S., Ashburner, J., Henson, R. N., Friston, K. J., & Frackowiak, R. S. (2001). A voxel-based morphometric study of ageing in 465 normal adult human brains. *NeuroImage*, 14(1 Pt. 1), 21–36. <http://doi.org/10.1006/nimg.2001.0786>
- Granger, C. W. J. (1969). Investigating causal relations by econometric models and cross-spectral methods. *Econometrica*, 37(3), 424. <http://doi.org/10.2307/1912791>

- Gregory, S., Long, J. D., Klöppel, S., Razi, A., Scheller, E., Minkova, L., ... Orth, M. (2018). Testing a longitudinal compensation model in pre-manifest Huntington's disease. *Brain*, 141, 2156–2166. <http://doi.org/10.1093/brain/awy122>
- Horwitz, B., Duara, R., & Rapoport, S. I. (1984). Intercorrelations of glucose metabolic rates between brain regions: Application to healthy males in a state of reduced sensory input. *Journal of Cerebral Blood Flow & Metabolism*, 4(4), 484–499. <http://doi.org/10.1038/jcbfm.1984.73>
- Jagust, W. J., Bandy, D., Chen, K., Foster, N. L., Landau, S. M., Mathis, C. A., ... Koeppe, R. A. (2010). The Alzheimer's disease neuro-imaging initiative positron emission tomography core. *Alzheimer's & Dementia*, 6(3), 221–229. <http://doi.org/10.1016/j.jalz.2010.03.003>
- Jiang, Y., Luo, C., Li, X., Duan, M., He, H., Chen, X., ... Yao, D. (2018). Progressive reduction in gray matter in patients with schizophrenia assessed with MR imaging by using causal network analysis. *Radiology*, 287(2), 633–642. <http://doi.org/10.1148/radiol.2017171832>
- Kuhl, D. E., Metter, E. J., Riege, W. H., & Phelps, M. E. (1982). Effects of human aging on patterns of local cerebral glucose utilization determined by the [<sup>18</sup>F] Fluorodeoxyglucose method. *Journal of Cerebral Blood Flow & Metabolism*, 2(2), 163–171. <http://doi.org/10.1038/jcbfm.1982.15>
- Lai, T.-J., Payne, M. E., Byrum, C. E., Steffens, D. C., & Krishnan, K. R. R. (2000). Reduction of orbital frontal cortex volume in geriatric depression. *Biological Psychiatry*, 48(10), 971–975. [http://doi.org/10.1016/S0006-3223\(00\)01042-8](http://doi.org/10.1016/S0006-3223(00)01042-8)
- Lerch, J. P., Worsley, K., Shaw, W. P., Greenstein, D. K., Lenroot, R. K., Giedd, J., & Evans, A. C. (2006). Mapping anatomical correlations across cerebral cortex (MACACC) using cortical thickness from MRI. *NeuroImage*, 31(3), 993–1003. <http://doi.org/10.1016/j.neuroimage.2006.01.042>
- Martin, A. J., Friston, K. J., Colebatch, J. G., & Frackowiak, R. S. J. (1991). Decreases in regional cerebral blood flow with normal aging. *Journal of Cerebral Blood Flow & Metabolism*, 11(4), 684–689. <http://doi.org/10.1038/jcbfm.1991.121>
- Mechelli, A., Friston, K. J., Frackowiak, R. S., & Price, C. J. (2005). Structural covariance in the human cortex. *The Journal of Neuroscience*, 25(36), 8303–8310. <http://doi.org/10.1523/JNEUROSCI.0357-05.2005>
- Metter, E. J., Riege, W. H., Kuhl, D. E., & Phelps, M. E. (1984). Cerebral metabolic relationships for selected brain regions in healthy adults. *Journal of Cerebral Blood Flow & Metabolism*, 4(1), 1–7. <http://doi.org/10.1038/jcbfm.1984.1>
- Prohovnik, I., Håkansson, K., & Risberg, J. (1980). Observations on the functional significance of regional cerebral blood flow in "resting" normal subjects. *Neuropsychologia*, 18(2), 203–217. [http://doi.org/10.1016/0028-3932\(80\)90066-4](http://doi.org/10.1016/0028-3932(80)90066-4)
- Reuter-Lorenz, P. A., & Park, D. C. (2014). How does it STAC up? Revisiting the scaffolding theory of aging and cognition. *Neuropsychology Review*, 24(3), 355–370. <http://doi.org/10.1007/s11065-014-9270-9>
- Ross, L. A., McCoy, D., Coslett, H. B., Olson, I. R., & Wolk, D. A. (2011). Improved proper name recall in aging after electrical stimulation of the anterior temporal lobes. *Frontiers in Aging Neuroscience*, 3, 16. <http://doi.org/10.3389/fnagi.2011.00016>
- Rousset, O. G., Ma, Y., & Evans, A. C. (1998). Correction for partial volume effects in PET: Principle and validation. *Journal of Nuclear Medicine*, 39(5), 904–911 Retrieved from <http://www.ncbi.nlm.nih.gov/pubmed/9591599>
- Rubin, T. N., Koyejo, O., Gorgolewski, K. J., Jones, M. N., Poldrack, R. A., & Yarkoni, T. (2017). Decoding brain activity using a large-scale probabilistic functional-anatomical atlas of human cognition. *PLoS Computational Biology*, 13(10), e1005649. <http://doi.org/10.1371/journal.pcbi.1005649>
- Salat, D. H., Buckner, R. L., Snyder, A. Z., Greve, D. N., Desikan, R. S. R., Busa, E., ... Fischl, B. (2004). Thinning of the cerebral cortex in aging. *Cerebral Cortex*, 14(7), 721–730. <http://doi.org/10.1093/cercor/bbh032>
- Shafiq, M. A., & Tyler, L. K. (2014). Language in the aging brain: The network dynamics of cognitive decline and preservation. *Science*, 346(6209), 583–587. <http://doi.org/10.1126/science.1254404>
- Smith, S. M., Miller, K. L., Salimi-Khorshidi, G., Webster, M., Beckmann, C. F., Nichols, T. E., ... Woolrich, M. W. (2011). Network modelling methods for FMRI. *NeuroImage*, 54(2), 875–891. Retrieved from <http://www.sciencedirect.com/science/article/pii/S1053811910011602>
- Smith, S. M., Vidaurre, D., Beckmann, C. F., Glasser, M. F., Jenkinson, M., Miller, K. L., ... Van Essen, D. C. (2013). Functional connectomics from resting-state fMRI. *Trends in Cognitive Sciences*, 17(12), 666–682. <http://doi.org/10.1016/j.tics.2013.09.016>
- Spreng, R. N., Wojtowicz, M., & Grady, C. L. (2010). Reliable differences in brain activity between young and old adults: A quantitative meta-analysis across multiple cognitive domains. *Neuroscience & Biobehavioral Reviews*, 34(8), 1178–1194. <http://doi.org/10.1016/j.neubiorev.2010.01.009>
- Tang, W., Bressler, S. L., Sylvester, C. M., Shulman, G. L., & Corbetta, M. (2012). Measuring Granger causality between cortical regions from voxelwise fMRI BOLD signals with LASSO. *PLoS Computational Biology*, 8(5), e1002513. <http://doi.org/10.1371/journal.pcbi.1002513>
- Taylor, P. A., Gohel, S., Di, X., Walter, M., & Biswal, B. B. (2012). Functional covariance networks: Obtaining resting-state networks from inter-subject variability. *Brain Connectivity*, 2(4), 203–217. <http://doi.org/10.1089/brain.2012.0095>
- Taylor, W. D., Steffens, D. C., McQuoid, D. R., Payne, M. E., Lee, S.-H., Lai, T.-J., & Krishnan, K. R. R. (2003). Smaller orbital frontal cortex volumes associated with functional disability in depressed elders. *Biological Psychiatry*, 53(2), 144–149. [http://doi.org/10.1016/S0006-3223\(02\)01490-7](http://doi.org/10.1016/S0006-3223(02)01490-7)
- Tibshirani, R. (1996). Regression selection and shrinkage via the lasso. *Journal of the Royal Statistical Society B*, 58(1), 267–288. <http://doi.org/10.2307/2346178>
- Yuan, R., Di, X., Kim, E. H., Barik, S., Rypma, B., & Biswal, B. B. (2013). Regional homogeneity of resting-state fMRI contributes to both neurovascular and task activation variations. *Magnetic Resonance Imaging*, 31(9), 1492–1500. <http://doi.org/10.1016/j.mri.2013.07.005>
- Zhang, Z., Liao, W., Xu, Q., Wei, W., Zhou, H. J., Sun, K., ... Lu, G. (2017). Hippocampus-associated causal network of structural covariance measuring structural damage progression in temporal lobe epilepsy. *Human Brain Mapping*, 38(2), 753–766. <http://doi.org/10.1002/hbm.23415>
- Zhang, Z., Liao, W., Zuo, X.-N., Wang, Z., Yuan, C., Jiao, Q., ... Liu, Y. (2011). Resting-state brain organization revealed by functional covariance networks. *PLoS One*, 6(12), e28817. <http://doi.org/10.1371/journal.pone.0028817>
- Ziegler, G., Penny, W. D., Ridgway, G. R., Ourselin, S., & Friston, K. J. (2015). Estimating anatomical trajectories with Bayesian mixed-effects modeling. *NeuroImage*, 121, 51–68. <http://doi.org/10.1016/j.neuroimage.2015.06.094>
- Ziegler, G., Ridgway, G. R., Blakemore, S.-J., Ashburner, J., & Penny, W. (2017). Multivariate dynamical modelling of structural change during development. *NeuroImage*, 147, 746–762. <http://doi.org/10.1016/j.neuroimage.2016.12.017>
- Zuendorf, G., Kerrouche, N., Herholz, K., & Baron, J.-C. (2003). Efficient principal component analysis for multivariate 3D voxel-based mapping of brain functional imaging data sets as applied to FDG-PET and normal aging. *Human Brain Mapping*, 18(1), 13–21. <http://doi.org/10.1002/hbm.10069>

## SUPPORTING INFORMATION

Additional supporting information may be found online in the Supporting Information section at the end of this article.

**How to cite this article:** Di X, Wölfer M, Amend M, et al. Interregional causal influences of brain metabolic activity reveal the spread of aging effects during normal aging. *Hum Brain Mapp*. 2019;40:4657–4668. <https://doi.org/10.1002/hbm.24728>